Structure and Function in Rhodopsin: Mapping Light-Dependent Changes in Distance between Residue 65 in Helix TM1 and Residues in the Sequence 306−319 at the Cytoplasmic End of Helix TM7 and in Helix H8[†]

Christian Altenbach,[‡] Kewen Cai,[§,||] Judith Klein-Seetharaman,[§,⊥] H. Gobind Khorana,*[,§] and Wayne L. Hubbell*[,‡]

Jules Stein Eye Institute and Department of Chemistry and Biochemistry, University of California, Los Angeles, California 90095-7008, and Departments of Biology and Chemistry, Massachusetts Institute of Technology, Cambridge, Massachusetts 02139

Received July 24, 2001; Revised Manuscript Received October 16, 2001

ABSTRACT: Spin-labeled double mutants of rhodopsin were produced containing a reference nitroxide at position 65, at the cytoplasmic termination of helix TM1, and a second nitroxide in the sequence of residues 306−319, which includes the cytoplasmic termination of helix TM7 and nearly the entire surface helix H8. Magnetic dipole−dipole interactions between the spins are analyzed to provide interspin distance distributions in both the dark and photoactivated states of rhodopsin. The distributions, apparently resulting from the conformational flexibility of the side chains, are found to be consistent with the structural model of rhodopsin in the dark state derived from crystallography. Photoactivation of the receptor triggers an increase in distance between residues in TM7, but not those in H8, relative to the reference at position 65 in TM1. The simplest interpretation of the result is a movement of the cytoplasmic portion of TM7 away from TM1 by 2−4 Å.

Site-directed spin labeling (SDSL)[1] has emerged as a powerful tool for the investigation of structure and dynamics in proteins of arbitrary molecular weight, both water-soluble and membrane-bound (for reviews, see refs *1*−*5*). In this method, substituted cysteine residues are modified with a sulfhydryl-selective reagent to provide a nitroxide side chain. In the studies presented here, the methanethiosulfonate reagent (I) was employed to produce the side chain designated R1 (Figure 1).

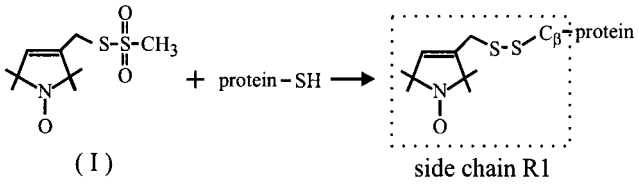

FIGURE 1: Reaction of methanethiosulfonate reagent I with a cysteine residue to yield side chain R1.

Two important quantities determined from the EPR of a single R1 in a folded protein are the solvent accessibility and mobility of the side chain. In previous studies, the sequence dependence of these quantities was used to deduce the secondary structure and salient features of the tertiary fold of the rhodopsin molecule throughout the entire cytoplasmic surface. In addition, changes were detected in the tertiary structure upon photoactivation that suggested relative movements of the TM helical segments (*6*−*16*).

In addition to the solvent accessibility and mobility, it is possible to estimate the interspin distance between two R1 side chains in a protein up to ∼20 Å using static or dynamic dipole−dipole interactions (*17*−*21*). In the study presented here, this capability is employed to map proximity relationships and to estimate the magnitude of light-activated helix movements in rhodopsin. The general strategy is to introduce one R1 residue at a "reference site" in the protein. A second R1 residue is then scanned through a sequence that lies nearby. The resulting set of distances relative to the reference provides a pattern that reflects the local structure. It is essential to obtain multiple sets of distances in this way to mitigate a potential bias due to the existence of multiple rotamers of the R1 side chain (*21*, *22*).

In previous experiments, distance mapping using double-spin-labeled rhodopsin was employed to estimate the amplitude of the light-activated movement of TM6 (*11*). In the study presented here, we investigate relative movements in

[†] Research reported here was supported by NIH Grants EY05216 (W.L.H.) and GM28289 and EY11716 (H.G.K.), the Jules Stein Professorship (W.L.H.), and a grant from the Bruce Ford Bundy and Anne Smith Bundy Foundation (W.L.H.). J.K.-S. was a recipient of a Howard Hughes Medical Institute Predoctoral Fellowship. This is paper 48 in the series Structure and Function of Rhodpsin.

* To whom correspondence should be addressed. W.L.H.: Jules Stein Eye Institute, UCLA School of Medicine, Los Angeles, CA 90095-7008; telephone, (310) 206-8830; fax, (310) 794-2144; e-mail, hubbellw@jsei.ucla.edu. H.G.K.: Departments of Chemistry and Biology, Massachusetts Institute of Technology, Cambridge, MA 02139; telephone, (617) 253-1871; fax, (617) 253-0533; e-mail, khorana@mit.edu.

[‡] University of California.

[§] Massachusetts Institute of Technology.

[||] Current address: Biogen, Inc., 14 Cambridge Center, Cambridge, MA 02142.

[⊥] Current address: Institute for Software Research International, Carnegie Mellon University, Wean Hall 4604, Pittsburgh, PA 15213.

[1] Abbreviations: DM, dodecyl maltoside; EPR, electron paramagnetic resonance; T4L, T4 lysozyme. Mutants with a single spin-label are designated by giving the sequence number for the spin-labeled position followed by R1. Thus, 65R1 is the mutant with the R1 side chain at site 65. Double-spin-labeled mutants are designated in a similar fashion; i.e., 65R1+306R1 is the double mutant with R1 side chains at sites 65 and 306.

10.1021/bi011546g CCC: $20.00
Published on Web 11/29/2001

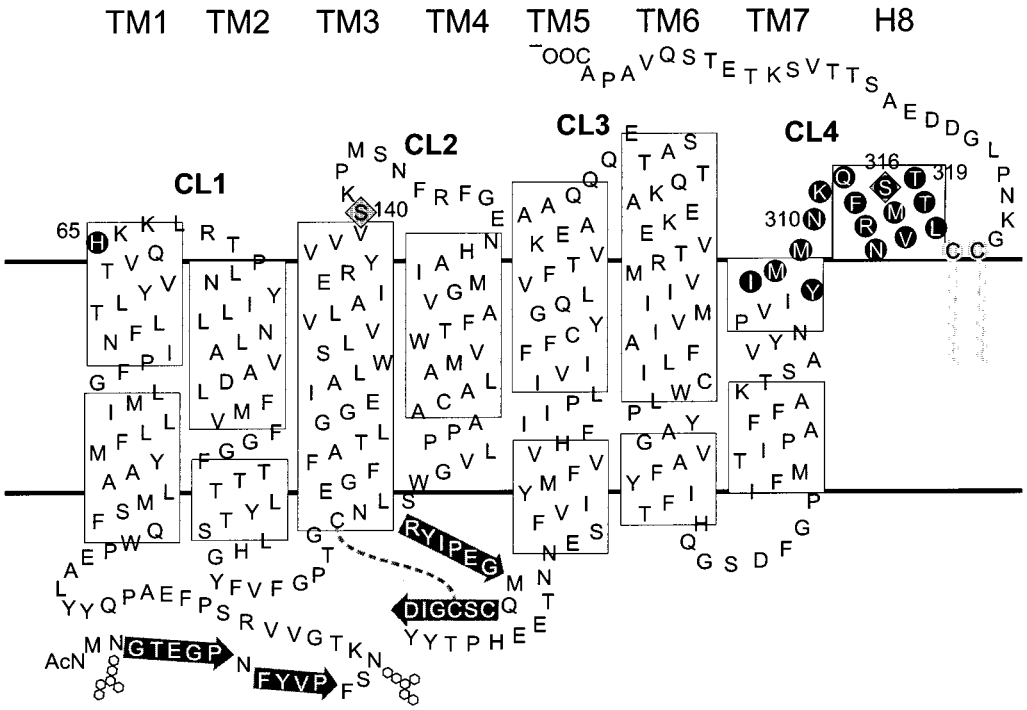

FIGURE 2: Secondary structural model of rhodopsin, highlighting the residues included in this study (black circles). The interhelical loops at the cytoplasmic surface are labeled CL1−CL4. Residue 65 at the cytoplasmic termination of TM1 was selected for substitution with one R1 side chain as a reference. A second R1 side chain was placed in the sequence of residues 306−319. Sites at which native cysteine residues were replaced with serine are indicated with diamonds. The secondary structure of CL3 is based on SDSL data (*9*), and that for the remainder of the molecule is derived from a crystal structure (PDB entry 1F88).

the TM1, TM7, H8 helix group. For this purpose, site 65 at the cytoplasmic termination of transmembrane helix TM1 is selected as a reference site, and a second R1 residue is placed at positions in the sequence of residues 306−319 that contains the cytoplasmic termination of TM7 (residues 306−310) and the short surface helix H8 that terminates at the palmitoylation sites 322 and 323 (Figure 2). Spin−spin interactions between the two nitroxides are analyzed from room-temperature data according to methods described in the preceding paper (*21*). The results show that residue 65 lies within spin−spin interaction range (<20 Å) of a number of residues in the sequence that was investigated. Modeling of the R1 side chain using conformations established from crystal structures of R1 in T4L (*22*) shows the consistency of the data with a structural model of rhodopsin derived from X-ray crystallographic data refined to 2.8 Å (*23*).

Photoactivation of rhodopsin results in detectable increases in distance between 65R1 and R1 residues throughout the sequence of residues 306−316, and between 310R1 and 316R1. The largest changes (2−4 Å) are between 310R1 and 316R1, and between 65R1 and R1 residues attached to the short helical segment comprised of residues 303−310. The pattern of changes suggests that this helical segment, lying just above the chromophore binding site, may move relative to neighboring structures upon photoactivation, perhaps in response to the motion of TM6 reported previously (*9*, *11*).

MATERIALS AND METHODS

Preparation and EPR Spectroscopy of Spin-Labeled Rhodopsin Mutants. The single-cysteine mutants of rhodopsin 65C, 306C, 308C−310C, 312C−316C, and 319C were prepared and purified in a DM (Anatrace, Maumee, OH) solution according to published procedures (*6*, *15*). The double-cysteine mutants containing 65C and a second cysteine at each of the positions listed above for the single mutants were prepared and purified in DM as described previously (*24*). In all cases, the purity of the preparations was high, with A_{280}/A_{500} spectral ratios in the range of 1.6−1.8. All single and double mutants were prepared in a base mutant of rhodopsin where reactive cysteines 140C and 316C were replaced with serine (Figure 2).

The single- and double-cysteine mutants in a DM solution were reacted with reagent I (Figure 1; a gift from K. Hideg, University of Pécs, Pécs, Hungary), and purified according to previously described methods (*6*). The labeled proteins in a DM solution were loaded into quartz capillaries under dim red light, and X-band EPR spectra were obtained using a loop-gap resonator as previously described (*25*). Following photobleaching as described previously (*9*), the EPR spectrum of the photoactivated form was recorded on the same sample and with identical instrument settings. Absorption EPR spectra were obtained by integration of the experimental first-derivative spectra after simple baseline and phase correction, where needed (*21*).

Analysis of EPR Spectra in Terms of Interspin Distances. Analysis of the spectra in terms of the interspin distance between nitroxide pairs in double mutants was carried out as described in the preceding paper (*21*). Briefly, the EPR spectrum of the double mutant is deconvoluted with the sum of the EPR spectra of the corresponding single mutants (the "noninteracting spectrum") to give a broadening function characteristic of the interaction. For dipole−dipole interaction between a pair of spins separated by a fixed distance and randomly oriented with respect to the magnetic field, the function is taken to be the so-called "Pake function" (*20*,

26). For a distribution of interspin distances, the broadening function is then a weighted sum of Pake functions.

Operationally, the experimentally determined broadening function is fit to a sum of Pake functions with the distance distribution as a parameter. The fit to the broadening function is then convoluted with the spectrum of the sum of the single mutants (the noninteracting spectrum) to provide a simulated spectrum. The agreement between the experimental and simulated spectrum is a measure of the validity of the derived distance distribution. This method holds for nitroxide−nitroxide interactions as long as (1) the nitroxide rings are oriented randomly with respect to one another, (2) the interspin vector is randomly oriented with respect to the external field, and (3) the interspin vector has a rotational correlation time τ_R of $\geq$20 ns.

The first condition is met if at least one of the sites is on the surface of the protein and mobile, where the ring occupies many orientations due to rotational isomerization about the two terminal bonds adjacent to the ring (*22*, *27*). This is the case for the studies presented here, where solvent-exposed mobile residue 65R1 is used as a common reference for all pairs (*6*). Moreover, the samples are solutions of rhodopsin in detergent, and the protein has no net orientation. Therefore, the second condition is fulfilled. Finally, the rotational correlation time of the interspin vector for a pair of nitroxides in rhodopsin is approximately the rotational correlation time of the protein itself. For rhodopsin in a DM micelle, the correlation time τ of the nitroxide is $\geq$30 ns, as deduced from the splitting of the hyperfine extrema and unaveraged *g* factor anisotropy in the most immobilized buried residues in rhodopsin in DM solutions (*10*); thus, the final condition is fulfilled.

Modeling of the Side Chains in Rhodopsin. To compare the experimentally measured distances with the structural model of rhodopsin (PDB entry 1F88), the R1 side chains were modeled pairwise in the structure, after replacing all other side chains with glycine, using the program Insight II [Accelrys (formerly MSI), San Diego, CA]. In addition, the rhodopsin structure was truncated beyond C323 (the C-terminal peptide). The C-terminal sequence has *B*-factors ranging from 60 to 90 in the crystal structure, and in solution is dynamically disordered beyond about P327 (*16*). The initial conformation for the R1 side chains was the favored g^+g^+ state observed in crystal structures (*22*). The dihedral of the disulfide (approximately $\pm$90), and X_4 and X_5 (the dihedral angles of the two bonds adjacent to the nitroxide ring) were manually adjusted to minimize steric overlap with main chain atoms. To search for a set of low-energy conformations that are consistent with the experimentally measured distances, the energy of the system was minimized in the Discover module of Insight II with respect to variation of only X_4 and X_5 in R1, keeping all other atoms fixed, and subject to the experimentally measured distances as constraints. The default force field (cvff) was used with electrostatic terms disabled. The main goal was minimization of atomic overlap.

RESULTS

EPR Spectra for the Double-Spin-Labeled Mutants and the Criteria for Spin−Spin Interaction. In analysis of dipole−dipole interactions between spin pairs, it is important that both cysteines be labeled as completely as possible. In a protein or mutants thereof containing no cysteines other than the introduced pair, this can be achieved by use of a large excess of reagent (I) and long reaction times. However, the base mutant of rhodopsin employed here contains native cysteines 167C, 185C, 222C, and 264C. Even though these sites are buried in the structure and are relatively unreactive, mild reaction conditions must be employed to avoid some labeling of these sites (*6*). Hence, modification of the introduced pair is not generally quantitative in rhodopsin, particularly when one or both of the sites are modestly reactive. The reference site mutant 65C is relatively reactive (*6*), but 307C, 317C, 318C, 320C, and 321C were previously found to be very slightly reactive (*13*), and these doubles were not investigated. In addition, double mutant 65R1/311R1 was not analyzed due to a very poor signal-to-noise ratio in the EPR spectrum. Figure 3 shows the first-derivative EPR absorption spectra for the remaining pairs in both the dark (solid trace) and photoactivated states (dashed trace).

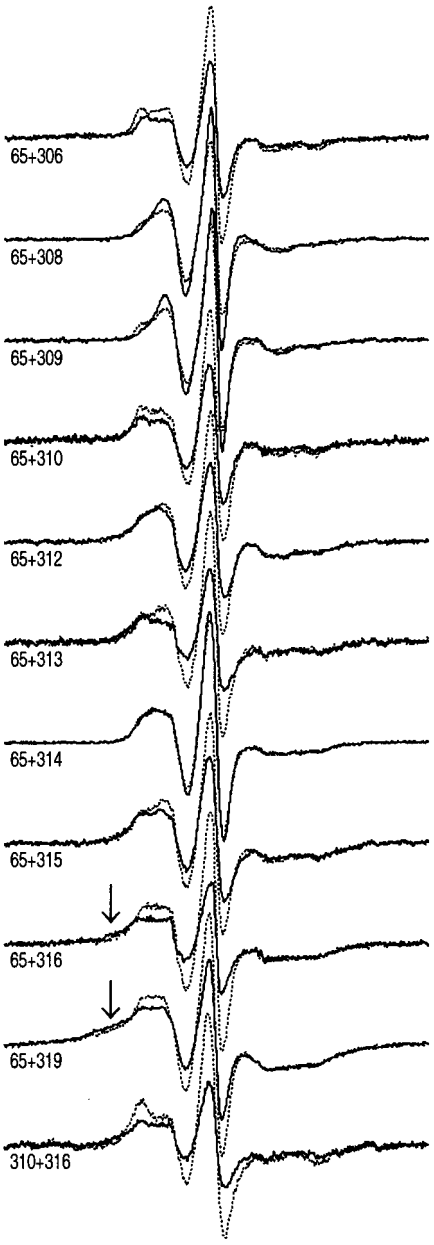

FIGURE 3: Experimental first-derivative EPR spectra of the double mutants in the dark (—) and after photoactivation (···).

Before one attempts quantitative analysis of the EPR spectra of the double-spin-labeled mutants, it is useful to establish criteria for positive identification of spin−spin interaction in the raw experimental data. Spin−spin interaction leads to spectral broadening of a degree dependent on the interspin distance. With near-quantitative labeling of both cysteine residues, strong spin−spin interaction is easily recognized by the overall breadth in the spectrum of the double mutant. For example, spin−spin interaction can be unequivocally detected by this criterion in the spectra for the interacting pairs 65R1 and 316R1, and 65R1 and 319R1, by the exaggerated "wings" in the spectra (Figure 3, arrows).

For the reasons discussed above, the labeling is often not quantitative. As a result, broadening due to a population of interacting spins in a significant background of noninteracting spins (due, for example, to some single-labeled protein) may be difficult to detect. This is because the noninteracting components are narrow and strongly dominate the intensity of the experimental first-derivative spectra. In such cases, rhodopsin offers a unique criterion for detecting spin−spin interaction in some pairs, namely, a light-dependent change in the intensity of the EPR spectrum of the double mutant, particularly in the central resonance line (Figure 3, difference between solid and dashed traces). Each of the spin-labeled sites employed here has been previously investigated as a single-spin-labeled mutant, and it was found that light activation of rhodopsin caused little change in the amplitude of the central resonance line (*6*, *13*). Thus, if a change in the EPR spectral amplitude is observed upon light activation of a rhodopsin double mutant, the change can be assigned to a modulation of spectral line width, and hence intensity, due to a change in spin−spin interaction. Examples of this effect have already been reported in rhodopsin (*10*, *11*). Since the dark and photoactivated spectrum was recorded on the same sample and with identical instrument settings, a photoactivation-dependent change in the central line intensity is a useful criterion for interaction, because it does not rely on any data manipulation such as integration, baseline corrections, etc. As can be appreciated in Figure 3, the light-activated changes in the EPR spectral amplitude for the pairs 65R1+306R1, 65R1+310R1, 65R1+312R1, 65R1+313R1, 65R1+316R1, 65R1+319R1, and 310R1+316R1 are particularly large (Figure 3a), and serve to identify spin−spin interactions, even though the broad interacting component is not easily detected in the first-derivative spectra of all of them due to the presence of a significant population of noninteracting spins. With this criterion, it is not possible to identify spin−spin interactions that are not modulated by light.

An underlying broad spectral population due to spin−spin interaction may be resolved from a sharper component more readily in the absorption spectra than in the conventional derivative spectra, particularly when compared to the corresponding noninteracting spectrum obtained as the average of the spectra of the corresponding single-spin-labeled mutants (*21*). As can be seen in Figure 4a (arrows), the spectra of 65R1+306R1 and 65R1+310R1 clearly have a broad underlying component, arising from a population of side chains with strong spin−spin interaction. The other sharper component could arise from either a single-labeled protein, or a population of spins with separations outside the detection limit. Figure 4b shows the corresponding comparison of the spectrum of the double-labeled mutant

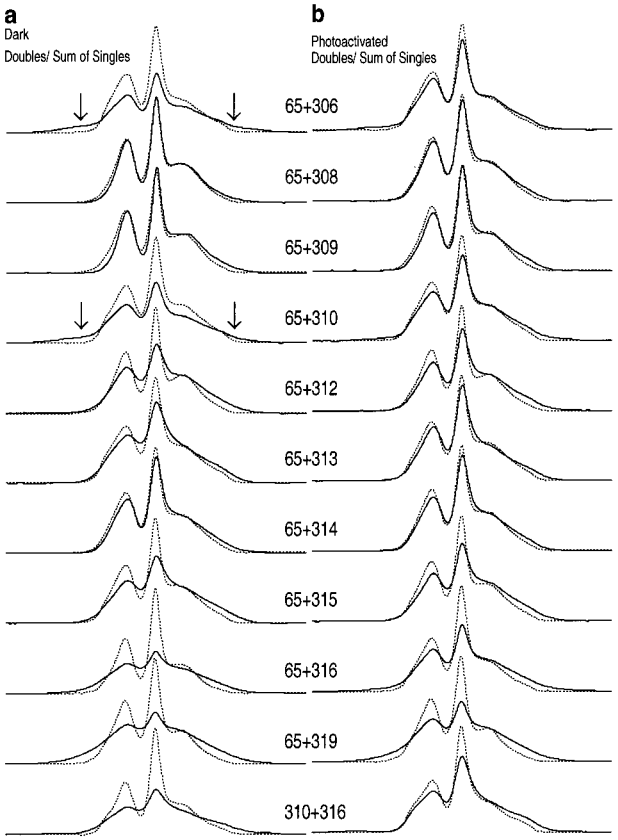

FIGURE 4: Absorption EPR spectra of R1 in rhodopsin. (a) Spectra of the indicated double mutant (—) and the algebraic sum of the corresponding single mutants (•••), both in the dark state. (b) Spectra of the indicated double mutant and the algebraic sum of the corresponding single mutants, both after photoactivation at room temperature. The absorption spectrum reveals the presence of broad, low-amplitude, underlying components that correspond to close distances in a distribution (denoted with arrows).

with that of the noninteracting spins in the light-activated state. For 65R1+306R1 and 65R1+310R1, the magnitude of the broad underlying component has decreased significantly and the spectra now more closely resemble the noninteracting state. For 65R1+315R1, 65R1+316R1, and 65R1+319R1, the broad component largely remains and the spin−spin interaction persists in the light-activated state.

Of the double-cysteine mutants studied here, 65R1+308R1, 65R1+309R1, and 65R1+314R1 yielded EPR spectra that had no broadening recognized by inspection, and were essentially independent of light activation (Figure 3). Moreover, the experimental spectra of the doubles are reasonably well represented by a 1:1 sum of the normalized spectra of the individual spin-labeled mutants (the noninteraction spectrum, Figure 4, dashed trace). This suggests that both sites are approximately equally labeled. Thus, it is tentatively concluded that both sites are labeled in these double mutants, and the lack of detectable broadening implies that they are >20 Å apart.

Analysis of Interacting Spin Pairs in Terms of Distance and Distance Changes with Photoactivation. In the paragraphs below, the interacting spin pairs identified by the above criteria, which include all but 65R1 with 308R1, 309R1, and 314R1, are analyzed in terms of interspin distance. For each spin pair identified as interacting, in either the dark or photoactivated state, the relative magnitude of

the spin−spin interaction can be qualitatively gauged directly from the data by the difference in the amplitude of the superposed spectra in Figure 4a or 4b, respectively, as discussed above. Similarly, relative changes in interaction upon photoactivation can be judged directly from Figure 3.

Quantitative interpretation of each interaction in terms of interspin distance distribution is possible using the deconvolution−convolution approach outlined in Materials and Methods and described in detail in the preceding paper (*21*). Panels a and b of Figure 5 summarize the results of such analyses in the dark and photoactivated states, respectively, in terms of the interspin distance distribution derived for the interacting pair. As a check on the validity of each distribution, the EPR spectrum simulated from the distribution (dashed trace) is compared with the experimental spectrum of the double mutant. First-derivative spectra are shown here because they provide a more critical assessment of the quality of the simulation than would be afforded by the absorption spectra. In each case, the simulated spectrum is in good agreement with the experimental spectrum of the double mutant. To achieve this result, it was necessary to include some fraction of noninteracting spins (f_{NI}), likely due to incomplete modification of the cysteines for the reasons mentioned above.

For the 65R1+306R1 double mutant, the distance distribution has one population in strong interaction at ~8 Å, and a smaller population at ~9 Å. The existence of strongly interacting spin pairs corresponding to the short distances is revealed by the broad component in the EPR absorption spectrum that is not present in the spectrum of the noninteracting spins (Figure 4a, arrow). The sharp noninteracting population ($f_{NI} = 0.24$) dominates the first-derivative spectrum (Figure 3, solid trace). Upon photoactivation, the increase in the amplitude of the EPR spectrum signals a decrease in the extent of interaction (Figure 3). Comparison of the distribution of interspin distances before and after activation suggests only a small (≈1 Å) increase in distance (Figure 4), but with an increase in f_{NI} of 0.28, a feature that is largely responsible for the intensity increase in the first-derivative spectra. Possible origins of this incremental noninteracting population will be discussed below.

The spectra for the double mutant 65R1+310R1 are very similar to those for 65R1+306R1. Residues 306R1 and 310R1 are both solvent-inaccessible (*13*) and face the interior of the protein, one helical turn apart (Figure 2). The derived distance distribution in the dark is bimodal with one mode at an interspin distance of ~7 Å and a second at ≈14 Å in a broad smear (and low amplitude; Figure 4a). Again, the noninteracting component ($f_{NI} = 0.32$) dominates the first-derivative EPR spectrum, but the strongly interacting population at 7 Å is evident in the broad wings of the absorption spectrum (Figure 4a, arrows). After photoactivation, the bimodal nature is more obvious. The distribution of distances in the activated state indicates populations with modes near 11 and 15 Å, suggesting a distance increase in the range of 4 Å for the more closely spaced population, and a narrowing of the distribution for the more widely spaced population (Figure 4b).

For 65R1+312R1, the apparent distribution of distances is unusually broad, extending from 10 to 20 Å with an f_{NI} of 0.18. The mode of the skewed distribution is near 12 Å, with a broad tail to longer distances. Upon photoactivation, the population near 12 Å changes little, but f_{NI} increases to 0.37, apparently due to a shift in the longer distances (14−18 Å) out of the range of interaction. This is responsible for the change in spectral intensity seen in Figure 3 upon photoactivation.

For 65R1+313R1, the data can be accounted for by essentially a single interspin distance near 12 Å with an f_{NI} of 0.6. With this large fraction of noninteracting spins, the experimental spectrum is strongly dominated by the more intense noninteracting population, and the distance and distribution are less reliable than for the other pairs. Light excitation reduces the extent of interaction, as for all sites (Figure 3). According to the distance distribution, there is an increase of ≈1 Å in the interspin distance, with an increase in the width of the distribution upon photoactivation, and little change in f_{NI}.

For 65R1+315R1, the distribution of distances is essentially bimodal with an f_{NI} of 0.22. One population has a relatively narrow distribution with the mode near 10 Å, and the other has a broad distribution (12−20 Å) with the mode at ≈15 Å. The distribution of distances in the photoactivated state indicates an increase in the interspin distance of ≈1 Å for the population at 10 Å, and an increase in the relative population of the longer distances. There is little change in f_{NI} upon photoactivation.

Strong spin−spin interaction in 65R1+316R1 in frozen solution has been previously reported (*10*). Analysis by the deconvolution−convolution method suggests a bimodal interspin distance distribution, with one mode at 9 Å (9 ± 2 Å), and the other at 13 Å. A low value for f_{NI} of 0.06 is consistent with the high reactivity of cysteine residues at these two sites. Light activation causes an increase in the distance of ≈1 Å for the major population at 9 Å, a shift of the other population to longer distances, and an increase in f_{NI} to 0.12.

The interaction between 65R1 and 319R1 is the strongest that has been seen, as can be appreciated by the spectral breadth (Figures 3 and 4a). Simulation of the spectrum requires a bimodal distribution, with one population sharply peaked around 8 Å, and the other around 11 Å, with an f_{NI} of 0.22. Light activation causes a negligible increase in the apparent interspin distance for the two populations seen in the dark, little change in f_{NI}, but the appearance of a small population of spins near the limit of detection (18 Å).

For 310R1+316R1, the distribution of interspin distances is again bimodal, with one mode sharply peaked around 11 Å and the other around 17 Å, with an f_{NI} of 0.14. After photoactivation, the interspin distance distribution is monomodal at 14 Å, with an f_{NI} of 0.32. This implies an increase in the interspin distance of ≈3 Å for the population at 11 Å, while the longer population moves out of the range of detection and contributes to the increase in f_{NI}.

Comparison of Experimental Inter-Residue Distances with the Rhodopsin Structural Model. Analysis of the spin−spin interaction in terms of interspin distance generally leads to the conclusion that there is a distribution of interspin distances, as shown in Figure 4. The origin of the distributions is almost certainly the conformational flexibility of the R1 side chain (*21*). Crystal structures of the R1 side chain at sites in α-helical sequences in T4L revealed three partial rotamers of the side chain classified as g^+g^+, tg^-, and g^+t depending on the X_1 and X_2 dihedral angles (*22*). Additional

rotamers exist depending on the values of X_3 (approximately ±90), X_4 (a wide range permitted in the absence of local interactions), and X_5 (approximately ±90). In each putative rotamer, including those involving X_3 and X_4, the nitroxide nitrogen atom lies approximately on a spherical surface ($r \sim 8$ Å), centered the R1 α-carbon, that subtends a solid angle of ~3 sr.

This potential conformational space was employed in comparing the derived distance distributions with predictions from the structural model of rhodopsin. Consistency with the structure was tested by determining if there is at least one set of rotamers in the allowed conformational space of R1 that simultaneously satisfies all the experimental interspin distances involving the single reference R1. This was done by modeling the reference 65R1 side chain and each secondary R1 side chain pairwise at the appropriate sites in the rhodopsin structure, after replacing all other side chains with glycine. Keeping the backbone atoms and the conformation of 65R1 fixed, we then minimized the energy of the system with respect to variation in the conformation of each secondary R1 residue, subject to the experimental distance constraints (see Materials and Methods). Replacing all side chains other than the spin-label with glycine avoids the necessity of repacking the local side chains to accommodate R1, and only R1 backbone interactions are thus considered.

In general, this procedure will identify sets of R1 conformations that are compatible with the experimental distance constraints, and accordingly, the data may be compatible with a set of different protein structures. Thus, it is only possible with this approach to eliminate incompatible structures. However, as the number of experimental distances increases, the number of compatible structures decreases sharply, and it is important to employ as many distances measurements as is feasible to map the structure.

Using the procedure described above, it is found that the interspin distances presented in Figure 5 are indeed consistent with both the rhodopsin structural model in the dark state and rotamers of the R1 side chains within the expected conformational space. For illustration, Figure 6 shows the structural model of rhodopsin with the R1 side chain modeled in configurations compatible with acceptable rotamers and experimentally determined interspin distances. For clarity, bimodal interspin distance distributions are represented only by the shortest distance modes (Figure 5). In these cases, populations corresponding to longer distance modes could be similarly modeled by rearrangement of the R1 conformations within the allowed conformational space (not shown).

In an earlier report, the distance between 65R1 and 316R1 in the dark state in frozen solution was estimated to be 10−13 Å by fitting the interacting spectra to a simple dipole−dipole interaction model assuming a Gaussian distribution of distances (*10*). This is in good agreement with the distance distribution reported here for the major population at room temperature (Figure 4).

DISCUSSION

Accessibility and Mobility of Residues 306R1−319R1 in Relation to the Rhodopsin Structure. In a previous SDSL study, a nitroxide scan was carried out through the sequence of residues 306−319 and the EPR spectra were analyzed to provide the solvent accessibility and mobility of the R1 residue at each site (*13*). These data identified 306R1, 310R1, and 313R1 as solvent-inaccessible and strongly immobilized, placing them within the protein interior. Moreover, the periodic dependence of the accessibility on sequence position identified the dominant regular secondary structure as an α-helix. These conclusions are confirmed by the structural model of rhodopsin derived from crystallographic data (*23*). The SDSL data on accessibility and mobility alone, however, were not sufficient to detect the change in the direction of the helical segment to form the short surface helix H8 (residues 311−322, Figure 2). Apparently, the face of helix H8 at which residues 314 and 318 reside is directly solvated by the bilayer. It is interesting that SDSL data do indeed identify 314R1 as one facing a fluid hydrophobic phase, judging from a high and low accessibility to collision with oxygen and NiEDDA, respectively (*13*). Residues 312R1, 315R1, and 319R1 define the solvent-exposed face of H8, and would be expected to be relatively highly mobile, characteristic of such sites (*28*). However, R1 at these sites has a population that is relatively immobilized, suggesting that this face of H8 experiences other interactions. In the crystal structure of rhodopsin, the C-terminal domain, beyond the palmitoylation sites at positions 322 and 323, is modeled with the segment of residues 324−327 along this face of H8, accounting for the additional interactions. This is also consistent with SDSL analysis of this domain, where R1 mobility reveals a partially ordered structure up to residue 326, but essentially complete disorder beyond (*16*).

In a previous study, residue 65R1 was shown to be solvent-exposed, and located at the cytoplasmic termination of TM1 ~10 Å from reside 316 in the dark state (*10*). This finding was particularly significant because these residues are at opposite ends of the sequence, and the result provided the first experimental evidence that the cytoplasmic terminations of TM1 and TM7 are in the proximity in the rhodopsin tertiary fold. In the studies presented here, we confirm that result for rhodopsin in solutions of DM at room temperature, and extend the study to include interactions between 65R1 and a second R1 in the sequence of residues 306−319. For all but three of the double-spin-labeled mutants that were analyzed, there is clear evidence of spin−spin interaction, placing the nitroxide residues within ~15 Å of each other.

Origin of the Distance Distributions. In a recent study of the interaction of spin pairs on T4L, the R1 sites were chosen to lie on the solvent-exposed surface of an α-helix, where the nitroxide group of R1 has little or relatively weak interaction with the environment (*21*). In that case, the distance distributions were narrow or bimodal and were interpreted to result from one or two thermally populated rotameric states of the side chain, as observed in crystal structures. For the spin pairs investigated in rhodopsin in this study, R1 is generally at regular helix sites, but may be located at solvent-inaccessible buried surfaces, solvent-accessible surface sites, or tertiary contact sites involving variable strengths of the interaction of the nitroxide ring with the environment. Apparently, the distribution of internitroxide distances depends on this structural context. For example, a single population of narrow width characterizes the distance distribution for interaction of 65R1 and buried, immobilized residues 306R1, 310R1, and 313R1. On the other hand, a broad, continuous distribution of distances is noted for pairs 65R1+312R1 and 65R1+315R1, while bimodal distributions

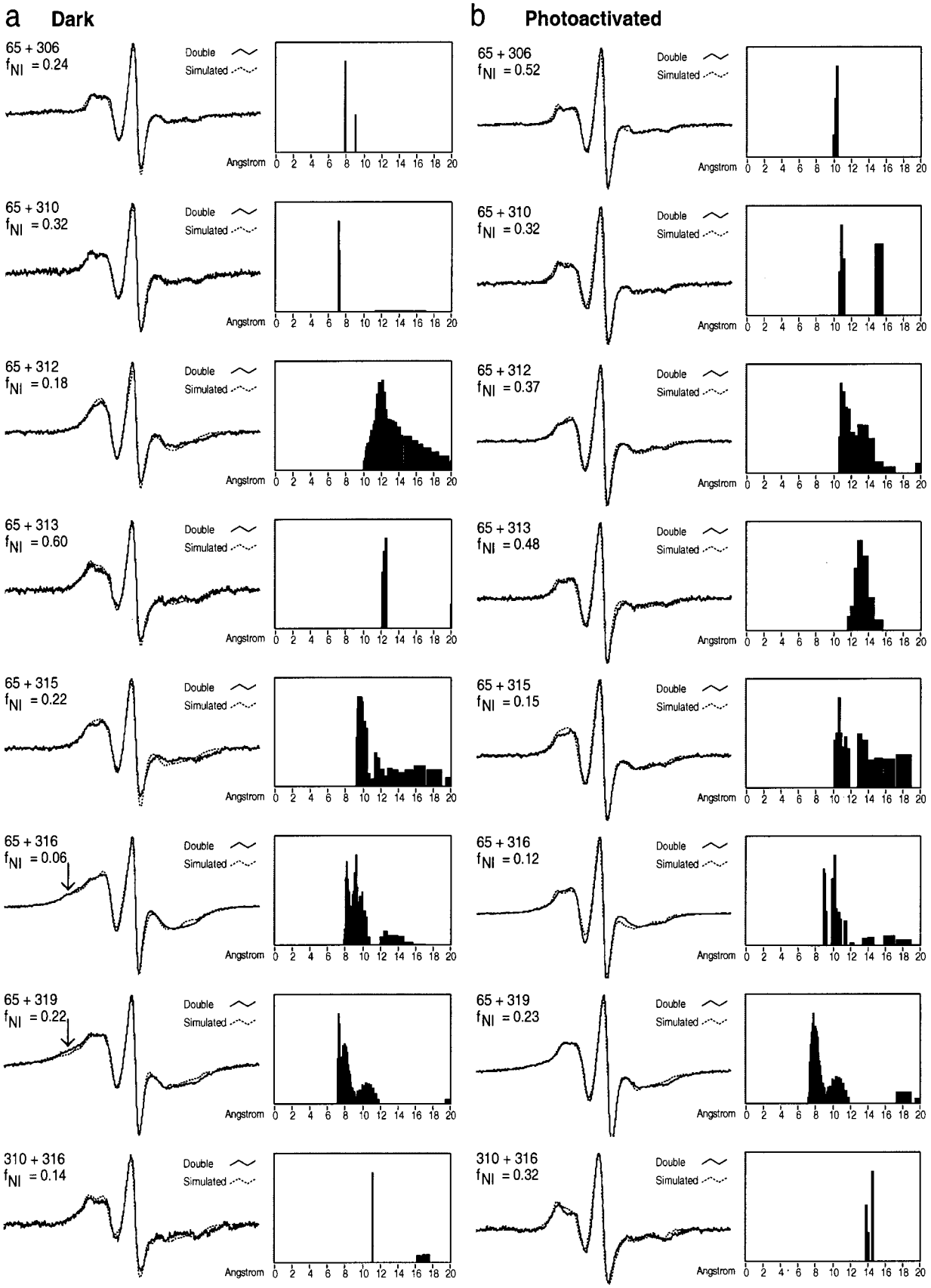

FIGURE 5: Experimental and simulated first-derivative EPR spectra and the derived interspin distance distribution for R1 spin pairs in rhodopsin. (a, left) Experimental first-derivative EPR spectrum of the indicated double mutant in the dark (—) and the simulated spectrum (···). (a, right) Derived distance distribution in the dark. (b, left) Experimental first-derivative EPR spectrum of the indicated double mutant in the light (—) and the simulated spectrum (···). (b, right) Distribution of distances after photoactivation. Only interacting spin pairs are included in the figure. The vertical (population) axes of the distributions are arbitrary and selected for convenience of display. The populations of spin pairs with inter-residue distances of >20 Å are not shown, but the fraction of total spin corresponding to these populations (f_{NI}) is given.

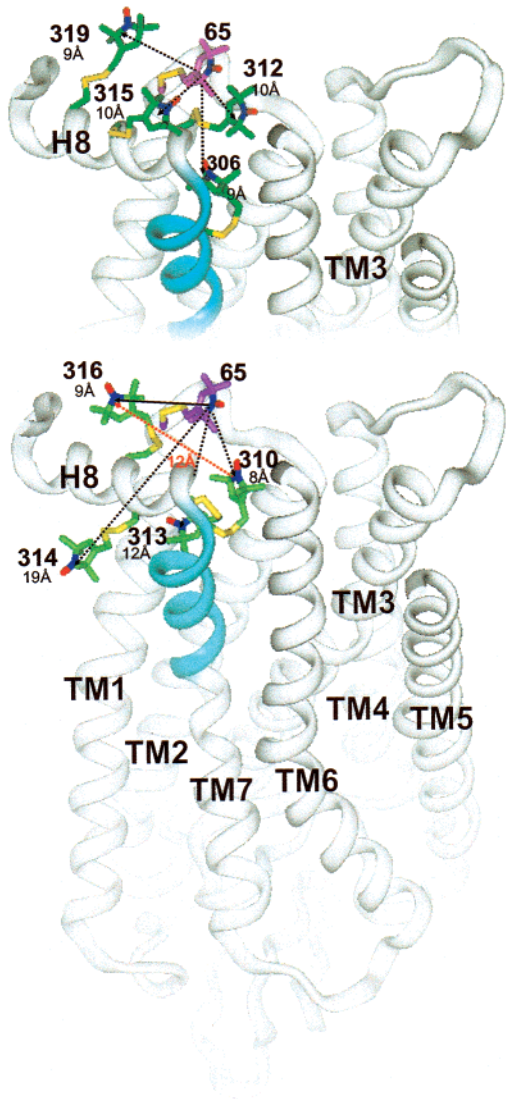

FIGURE 6: Ribbon models of rhodopsin based on a crystal structure (PDB entry 1F88) showing the locations of R1 side chain pairs as stick models. The reference 65R1 is highlighted in blue. The R1 side chains shown are in energy-minimized conformations that account for the experimental distances.

are the case for 65R1+316R1 and 65R1+319R1. This striking difference in distribution may result from differences in the degree of interaction of the side chain with the protein. For example, the single-spin-labeled mutants 312R1, 315R1, 316R1, and 319R1 all have multicomponent spectra indicative of tertiary contact interactions (*13*). For 312R1, 315R1, and 319R1, these interactions are likely to be with the C-terminal domain, as mentioned above. Such interactions could modulate the relative energies of various R1 rotamers (*22*), leading to additional conformations not observed at noninteracting surface sites. Consequently, there may be a broad or bimodal distribution of interspin distances between pairs of such nitroxides. At buried sites, strong packing interactions can easily be imagined to impose a single conformation on the R1 side chain.

As noted above, each distribution is accompanied by a population of apparently noninteracting spins. In principle, this could arise from (1) a partially unfolded population of rhodopsin (or a second conformation), (2) the existence of multiple rotamer states of R1, some of which result in separations of ≥20 Å, or (3) incompletely labeled protein. The first is unlikely because the A_{280}/A_{500} absorbance ratio in the UV−visible absorption spectrum was in the range of 1.6−1.8, for all mutants, indicating a highly pure folded protein. In addition, the EPR spectra of many of the single-spin-labeled mutants indicate a homogeneous environment. The second option is possible in particular cases, but the third is considered most likely for the reasons discussed above.

Effects of Photoactivation upon Inter-Residue Distances. Upon photoactivation, there are small but detectable shifts in the interspin distance for several of the spin pairs studied here. In addition, three of the spin pairs (65R1+306R1, 65R1+312R1, and 310R1+316R1) show significant increases (ca. 20%) in a population of noninteracting spin (r > 20 Å). The noninteracting population in the dark state is believed to arise predominantly from single-labeled protein, but the origin of the *increase* in this population upon photoactivation is unknown; however, it could arise from two likely sources. First, the population of interacting spins at long distances increases slowly with time (over the course of ≈30 min) in DM following the initial photoactivation. Because exposure to light and subsequent signal averaging takes a few minutes to complete, the incremental noninteracting population may represent decay to other photointermediates (*6*), or possibly some local unfolding. Alternatively, a new population of noninteracting spins could arise due to the formation of rotamers of one or both side chains that correspond to interspin distances outside the range of spin−spin interaction. Such a shift in rotamer populations could be induced by changes in side chain local packing interactions. Given the broad conformational space of the R1 side chain, this could account for the observed changes. In either case, the distance changes between the populations shown in Figure 4 are deemed the most relevant for inferring structural changes in the protein backbone during photoactivation to the MII state, and these are discussed below.

Upon photoactivation, there is little change in the distribution of the interspin distance in 65R1+319R1, and the distribution of distances in 65R1+316R1 and 65R1+312R1 shifts by only ∼1−2 Å, although the tail of the broad distribution involving 312R1 moves outside the interaction range. It is possible that this latter effect reflects some movement in the C-terminal tail, which apparently contacts 312R1 (see above). Taken together, the data suggest that there is little relative movement between the cytoplasmic end of helix TM1 and the surface helix H8 (residues 311−319) induced by photoactivation. In an earlier report, spectra of dark and photoactivated 65R1+316R1 obtained in frozen solutions were interpreted by fitting to a simple dipole−dipole interaction model with a Gaussian distribution of distances (*10*). As mentioned above, the average distance obtained in the dark agreed well with that reported here. However, the change in distance upon photoactivation was ≈5 Å compared to the value of 1−2 Å found here. The difference may be due to the use of frozen solutions in the earlier work or the more simplified analysis employed then.

The most significant changes in interspin distance distributions upon photoactivation are for pairs 65R1+306R1, 65R1+310R1, and 310R1+316R1. Because there is little change in the interspin distance between 65R1 and residues in helix H8, it seems unlikely that the changes in 65R1+306R1

and 65R1+310R1 are due to a relative displacement of 65R1. Rather, light-activated motions of 306R1 and 310R1 would provide a consistent explanation of the data. There are two possible causes for the movement of these residues. First, note that both 306R1 and 310R1 are immobilized and solvent-inaccessible in the protein core (*13*), and occupy a region of space in the proximity of the surface of contact with transmembrane helix TM6. In previous studies, it was shown that light activation causes a large amplitude outward movement of helix TM6 as a rigid body (*11*). Thus, it is possible that residues 306R1 and 310R1 change conformation in response to local repacking of the protein core induced by helix TM6 motion. In this case, the experimentally measured distance change would arise from side chain motions rather than exclusively from backbone motions.

A more attractive mechanism for the light-activated increase in the interspin distance in pairs 65R1+306R1, 65R1+310R1, and 310R1+316R1 is movement of the short helical segment (residues 302−209, violet in Figure 6) lying just above the retinylidene-protonated Schiff base linkage to K296. Such movement could in turn be induced either by the concerted movement of helices TM6 and TM7 or by the displacement of the backbone during the deprotonation of the Schiff base during the formation of metarhodopsin II (*29*).

Correlation between Disulfide Cross-Linking Rates and SDSL Distance Measurements. In general, there is quite good agreement between the proximity measured by SDSL and that inferred from the disulfide cross-linking rates reported previously (*24*). Thus, the most rapidly cross-linking mutants H65C+N315C and H65C+316C are also those showing strong interaction between attached nitroxides. Likewise, other mutants that show measurable cross-linking rates, namely, 65C+310C, 65C+312C, and 65C+313C, also exhibit clear spin−spin interaction when spin-labeled. Two differences stand out, and these can be attributed to the very different requirements for spin−spin interaction and disulfide cross-linking (*24*, *30*). First, 65R1+319R1 has the strongest spin−spin interaction but exhibits no cross-linking. This may be accounted for by the apparent rigidity of the rhodopsin structure in the region of residues 317−321 and the interaction with the C-terminal tail. Thus, even though residues 65 and 319 may be in proximity, the local structure may not permit the relaxation or fluctuation necessary to achieve the proper relative orientations to form the disulfide bond. Second, 65R1+306R1 exhibits a detectable interaction, but no cross-linking is observed. This may again be due to the rigid nature of the structure in this region, preventing residue 65C at the micelle−aqueous interface from contacting 306C that is ∼5 Å deep in the protein interior. On the other hand, the poor cross-linking could arise from the intrinsically low reactivity of the SH group of 306C as found in an earlier study (*15*).

SUMMARY AND CONCLUSIONS

The studies presented here and in the following paper (*31*) are the first applications of nitroxide−nitroxide distance estimation at room temperature in mapping structure and structure changes in rhodopsin. The broad distance distributions observed for pairs of R1 residues involving a tertiary contact site probably arise from multiple rotameric states stabilized by the interactions themselves. Interestingly, the distance distributions involving 65R1 and R1 at a buried site are relatively narrow, possibly due to the selection of a single rotamer by strong packing interactions. Due to the generally broad distributions, distance measurements using R1 are limited to testing a structural model for consistency with the data. In the region investigated here, the data are found to be entirely consistent with the structural model of rhodopsin derived from crystallographic studies. Upon photoactivation, little relative movement is detected between helices TM1 and H8, but relative motions on the order of 2−4 Å are inferred between 65R1 in the cytoplasmic termini of helix TM1 and R1 residues in TM7. However, these movements are small compared to those previously reported for helix TM6 relative to helix TM3 (*11*).

REFERENCES

1. Hubbell, W., and Altenbach, C. (1994) *Curr. Opin. Struct. Biol. 4*, 566−573.
2. Hubbell, W. L., Mchaourab, H., Altenbach, C., and Lietzow, M. A. (1996) *Structure 4*, 779−783.
3. Hubbell, W. L., Gross, A., Langen, R., and Lietzow, M. A. (1998) *Curr. Opin. Struct. Biol. 8*, 649−656.
4. Feix, J. B., and Klug, C. S. (1998) in *Biological Magnetic Resonance. Volume 14: Spin Labeling: The Next Millenium* (Berliner, L. J., Ed.) pp 251−281, Plenum Press, New York.
5. Hubbell, W. L., Cafiso, D. S., and Altenbach, C. (2000) *Nat. Struct. Biol. 7*, 735−739.
6. Resek, J. F., Farahbakhsh, Z. T., Hubbell, W. L., and Khorana, H. G. (1993) *Biochemistry 32*, 12025−12031.
7. Farabakhsh, Z., Hideg, K., and Hubbell, W. L. (1993) *Science 262*, 1416−1419.
8. Farahbakhsh, Z. T., Ridge, K. D, Khorana, H. G., and Hubbell, W. L. (1995) *Biochemistry 34*, 8812−8819.
9. Altenbach, C., Yang, K., Farrens, D. L., Farahbakhsh, Z. T., Khorana, H. G., and Hubbell, W. L. (1996) *Biochemistry 35*, 12470−12478.
10. Yang, K., Farrens, D. L., Hubbell, W. L., and Khorana, H. G. (1996) *Biochemistry 35*, 12464−12469.
11. Farrens, D. L., Altenbach, C., Yang, K., Hubbell, W. L., and Khorana, H. G. (1996) *Science 274*, 768−770.
12. Cai, K., Langen, R., Hubbell, W. L., and Khorana, H. G. (1997) *Proc. Natl. Acad. Sci. U.S.A. 94*, 14267−14272.
13. Altenbach, C., Cai, K., Khorana, H. G., and Hubbell, W. L. (1999) *Biochemistry 38*, 7931−7937.
14. Altenbach, C., Klein-Seetharaman, J., Hwa, J., Khorana, H. G., and Hubbell, W. (1999) *Biochemistry 38*, 7945−7949.
15. Cai, K., Klein-Seetharaman, J., Farrens, D., Zhang, C., Altenbach, C., Hubbell, W. L., and Khorana, H. G. (1999) *Biochemistry 38*, 7925−7930.
16. Langen, R., Cai, K., Altenbach, C., Khorana, H. G., and Hubbell, W. L. (1999) *Biochemistry 38*, 7918−7924.
17. Likhtenstein, G. I. (1976) *Spin Labeling Methods in Molecular Biology*, Chapter 3, John Wiley and Sons, New York.
18. Steinhoff, H. J., Radzwill, N., Thevis, W., Lenz, V., Brandenburg, D., Antson, A., Dodson, G., and Wollmer, A. (1997) *Biophys. J. 73*, 3287−3298.
19. Hustedt, E. J., Smirnov, A. I., Laub, C. F., Cobb, C. E., and Beth, A. H. (1997) *Biophys. J. 74*, 1881−1887.
20. Rabenstein, M. D., and Shin, Y.-K. (1995) *Proc. Natl. Acad. Sci. U.S.A. 92*, 8239−8243.
21. Altenbach, C., Oh, K.-J., Trabanino, R. J., Hideg, K., and Hubbell, W. L. (2001) *Biochemistry 40*, 15471−15482..
22. Langen, R., Oh, K.-J., Cascio, D., and Hubbell, W. L. (2000) *Biochemistry 39*, 8396−8405.
23. Palczewski, K., Kumasaka, T., Hori, T., Behnke, C. A., Motoshima, H., Fox, B. A., Le Trong, I., Teller, D. C., et al. (2000) *Science 289*, 739−745.
24. Cai, K., Klein-Seetharaman, J., Altenbach, C., Hubbell, W., and Khorana, H. G. (2001) *Biochemistry 40*, 12479−12485.
25. Altenbach, C., Flitsch, S., Khorana, H. G., and Hubbell, W. L. (1989) *Biochemistry 28*, 7806−7812.

26. Pake, G. E. (1948) *J. Chem. Phys. 16*, 327−336.
27. Columbus, L., Kálai, T., Jekö, J., Hideg, K., and Hubbell, W. L. (2001) *Biochemistry 40*, 3828−3846.
28. Mchaourab, H. S., Lietzow, M. A., Hideg, K., and Hubbell, W. L. (1996) *Biochemistry 35*, 7692−7704.
29. Lewis, J. W., and Kliger, D. S. (2000) *Methods Enzymol. 315*, 164−178.
30. Klein-Seetharaman, J., Cai, K., Altenbach, C., Hubbell, W. L., and Khorana, H. G. (2001) *Biochemistry 40* (in press).
31. Altenbach, C., Klein-Seetharaman, J., Cai, K., Khorana, H. G., and Hubbell, W. L. (2001) *Biochemistry 40*, 15493−15500.

BI011546G